IEEE Photonics Journal
An IEEE Photonics Society Publication

All-Optical Wavelength Multicasting in Quadruple Resonance-Split Coupled Silicon Microring Cavity

Volume 10, Number 6, December 2018

Awanish Pandey, *Member, IEEE*
Shankar Kumar Selvaraja, *Senior Member, IEEE*

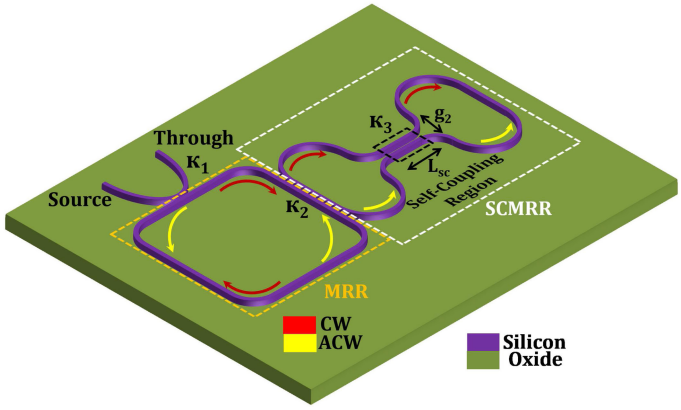

DOI: 10.1109/JPHOT.2018.2879594
1943-0655 © 2017 IEEE

All-Optical Wavelength Multicasting in Quadruple Resonance-Split Coupled Silicon Microring Cavity

Awanish Pandey, ***Member, IEEE***,
and Shankar Kumar Selvaraja, ***Senior Member, IEEE***

Centre for Nano Science and Engineering, Indian Institute of Science, Bengaluru 560012, India

DOI:10.1109/JPHOT.2018.2879594

Manuscript received May 24, 2018; revised October 9, 2008; accepted October 22, 2018. Date of publication November 5, 2018; date of current version November 22, 2018. The work of A. Pandey was supported by the Sir Visvesvaraya Fellowship, MeitY, Government of India. The work of S. K. Selvaraja was supported by the Sir Visvesvaraya Faculty Fellowship. This work was supported in part by MHRD, in part by MeitY, and in part by DST Nano Mission. Corresponding author: Shankar Kumar Selvaraja (e-mail: shankarks@iisc.ac.in).

Abstract: We demonstrate an all-optical four-channel wavelength multicasting in a coupled silicon microring resonator system. The scheme is based on two-photon-absorption-induced free carrier dispersion in silicon. The coupled cavity facilitates resonance splitting that is utilized as individual channels for multicasting. Using the split resonances, we achieve an aggregate multicasted data rate of 48 Gbps (4 $\times$ 12 Gbps). Moreover, we also present a detailed analysis and performance of the multicasting architecture using bit error rate and eye diagram measurements.

Index Terms: Silicon-on-insulator, photonic integrated circuits, cavity resonators.

1. Introduction

Wavelength multicasting is an essential functionality in optical networks that facilitates efficient and simultaneous routing of information from a single source to desired multiple recipients [1]–[3]. It involves replicating an input optical signal onto many different wavelengths and hence enabling data to be simultaneously forwarded to more than one recipient. Moreover, multicasting can also be employed to accomplish several other signal processing appliations such as radio frequency reciever [4] and tapped delay lines [5].

Silicon photonics based on-chip optical methods have emerged as a promising candidate for multicasting. They offer most compact and economical solution combined with multitudes of functionality compared to other competing platforms like wavelength selective switches and micro-opto-electro-mechanical systems (MOEMS) [6]. Despite weak non-linear properties of Si; low propagation loss, high light confinement and power density in Si waveguides allows enhanced non-linear interactions even at relatively low power levels that can be exploited for various non-linear optical applications [7]. Wavelength multicasting has been demonstrated using Si wire waveguides utilising different non-linear processes like cross-phase modulation [8], four wave mixing in Si, SOA and fiber [9]–[12] and also in different hybrid Si platforms like Indium-Phosphide-on-Si waveguides [13]. In all the above demonstrations, Si platfrom uses dispersion engineered long Si waveguides. The

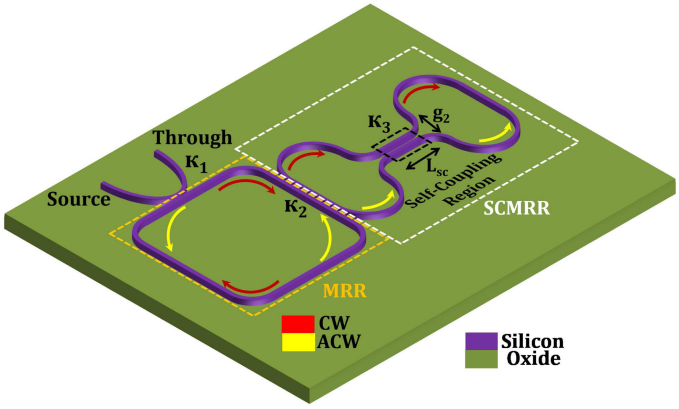

Fig. 1. Schematic of the proposed coupled resonator.

effect of non-linearity in Si waveguides can be enhanced by using resonant structures like microring resonators (MRRs). The intensity build-up in MRRs lowers the power requirement even more so that non-linear effects can be achieved for optical power in the waveguide as low as 3 mW [14]. Multicasting has also been demonstrated using MRRs where the resonance shift is achieved through Free Carrier Dispersion (FCD) [15], [16]. Free carriers are generated at MRR resonance wavelength as a consequence of two−photon absorption (TPA) in Silicon. This leads to Free Carrier Dispersion (FCD) that can then be utilised to attain multicasting via MRR resonances [16]. TPA based FCD in Silicon has been studied in detail for waveguides as well as resonators to study the dynamic behaviour of spectral response as well as utlizing it for variety of applications [17]–[20].

Since MRR resonances act as multicasting channels, it becomes necessary to have small Free Spectral Range (FSR) to enhance the number of channels. However, the inverse relationship between cavity size and FSR mandates MRR to have large geometrical length. Such designs not only compromises the compactness of cavity but also renders it susceptible towards propagation loss. We have earlier shown that splitting the resonances is a potential solution where a cavity resonance could be selectively splitted into closely spaced resonances [21]. Such splitting of resonances have already been demonstrated and utilized in areas like photonic links, differential-equation solver and microwave photonics [22]–[25]. In this paper, we propose a coupled cavity system that can split a cavity resonance into four closely spaced sub-resonances. We demonstrate four channel wavelength multicasting by transmitting data at 12 Gbps per channel and an aggregate data rate of 48 Gbps. We report comprehensive simulation and experimental analysis of the proposed structure and analyse the quality of multicasting channels using eye diagram and bit error rate analysis.

2. Structure and Working Principle

The schematic of the proposed coupled cavity system is shown in Fig. 1. It is an assembly of a conventional MRR externally loaded with a Self−Coupled MRR (SCMRR). A detailed discussion on the design and working principle of the SCMRR is presented in [21]. A typical MRR has mode propagating in either clockwise or anti-clockwise direction and resonates at wavelengths that phase match with the cavity. However, SCMRR has the ability to excite both clockwise and anti-clockwise propagating modes simultaneously due to the addition of a Self-Coupling Region (SCR) in the structure (Fig. 1). Interference between these two modes results in a split of the resonances. The SCMRR self-coupling co-efficient κ_3 can control the spacing between the resonances. A simple MRR coupled to another MRR can also split the resonance when phase matched [26]. The coupled MRR introduces optical path length difference between the single MRR mode and combined cavity hybrid mode and depending on the path length difference; selective resonances can be split. In our design, we achieve both types of splitting simultaneously, resulting in four cavity resonances by coupling a conventional MRR to a SCMRR.

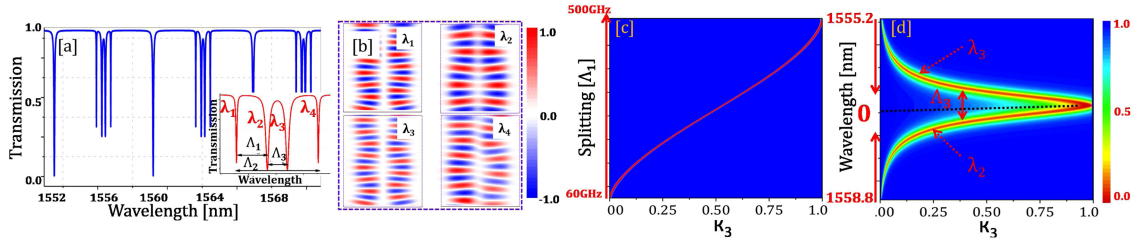

Fig. 2. Simulation results summary. (a) Transmission spectra of the proposed cavity. (b) Field distribution in the self-coupling region at four split wavelengths. (c) and (d) Variation of Λ_1 and Λ_3 respectively with κ_3.

Simulated results of the proposed coupled cavity are shown in Fig. 2. The circumference of the SCMRR (87 μm) was chosen to be half of the MRR (174 μm). A coupling length of 10 μm between MRR and SCMRR is chosen to allows phase matching of alternate resonances of MRR with SCMRR. As shown in Fig. 2(a), alternate resonances have undergone quadruple splitting at wavelengths λ_1, λ_2, λ_3 and λ_4 whereas other resonances are unperturbed. Here, we define FSR as the distance between resonances of MRR when it not coupled to SCMRR ($\kappa_2 = 0$). The splitting is characterized by calculating Λ_1, Λ_2 and Λ_3 as shown in the inset of Fig. 2(a). Fig. 2(b) shows a 2D-FDTD simulation of the field distribution in the coupling region. The fields are observed to have an anti-symmetric coupling at λ_1 and λ_3 whereas symmetric coupling at λ_2 and λ_4. The conjugate symmetric and anti-symmetric field distribution at successive split wavelengths confirms that the splitting arises due to interference between two contra-propagating degenerate resonant modes of the cavity [27]. As mentioned earlier, self-coupling in SCMRR plays a crucial role in resonance splitting. Fig. 2(c) and 2(d) show the effect of κ_3 on Λ_1 and Λ_3. For $\kappa_3 = 0$, Λ_1 is entirely from co-propagating SCMRR mode interference (60 GHz). As the power in anti-clockwise mode is increased by increasing κ_3 the splitting starts to increase as shown in Fig. 2(c) and becomes equal to 500 GHz at $\kappa_3 = 1$, which is the FSR of the MRR. The Λ_3, however, shows a decreasing trend with κ_3 and reaches 0 for $\kappa_3 = 1$ as shown in Fig. 2(d). It is worth noting that at $\kappa_3 = 1$, SCMRR imparts an additional π phase shift at the SCR and as a result the entire spectrum of the coupled cavity shifts by FSR/2.

The proposed coupled cavity structure was patterned on a Silicon-On-Insulator wafer with 220 nm Si layer and 2 μm thick buried oxide using electron-beam lithography, and dry etch process. The pattern in the resist is transferred into 220 nm Si layer using a Fluorine based chemistry using an inductive coupled plasma dry etch process. Grating fiber-chip couplers were fabricated to couple the light in and out of the device.

The spectral response of the fabricated device is shown in Fig. 3(a). The measurements were performed using a tunable laser and a power meter. The device spectrum is normalized with the response of a straight waveguide to calculate the insertion loss of the device. We measure a grating coupler loss and device insertion loss of 5 dB/coupler and 1.9 dB respectively. The device shows an alternate pattern of split resonance as discussed earlier. Fig. 3(b) shows the unperturbed and splitting response of the fabricated device. However, at higher wavelengths we observe splitting of the unperturbed as well (Fig. 3(c)). We attribute this splitting to reflection at the MRR-SCMRR coupling region. Since the coupling length between MRR and SCMRR is 10 μm, the linewidth variation of the waveguides increases the back-reflections at higher wavelengths. The mode size becomes larger that could excites a counter-propagating mode from the MRR-SCMRR coupling region. The counter-propagating modes can split the MRR resonances that are not phase-matched with SCMRR as highlighted in Fig. 3(c)

As previously discussed, the spacing between the split resonances can be varied by tuning the κ_3 of the SCMRR. Fig. 3(d) depicts the evolution of the splitting; Λ_1 and Λ_3, with κ_3. We observe an increase in Λ_1 from 180 GHz to 220 GHz while Λ_3 decreases from 165 GHz to 70 GHz for κ_3 variation of 12%, which matched well with our simulation (Fig. 2). When the signal wavelength

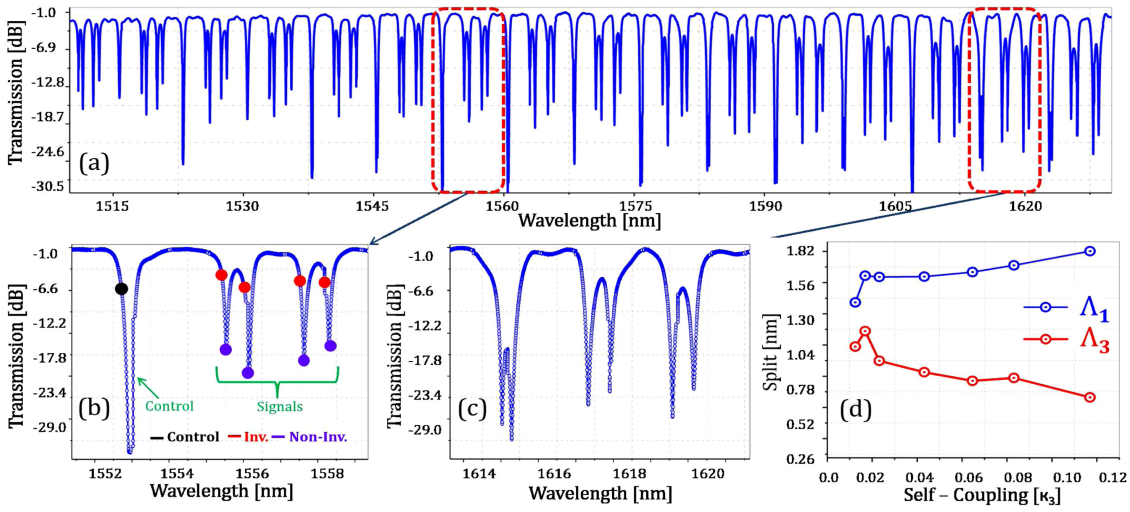

Fig. 3. (a) Spectral transmission curve of coupled cavity system. (b) Placement of control and signal wavelengths for multicasting. (c) Splitting of unperturbed resonances due to non-ideal coupling between MRR and SCMRR. (d) Variation of splitting with different κ_3.

is parked at the split resonances and the modulated control (with NRZ random bits) at the slope of the unperturbed resonance, a non-inverted multicasting is obtained (Fig. 3(b) purple dots). If the control carries a bit '1', free carriers are generated in Si that decreases the effective index. The FCD induced decrease in effective index blue shifts the resonance which in turn increases the transmission of the signal. In this way bit '1' is passed as a bit '1' and since bit '0' will not generate any free carrier, the signal will remain aligned with resonance and hence passed as bit '0'. However, when the signals are aligned at the slope of the split resonances as shown in Fig. 3(b) (red dots), the scheme would generate an inverted signal. Bit '1' induces blue shift and aligns the signal to the resonance dip whereas bit '0' keeps the alignment of signal on the slope. It results in inversion of the bit pattern, and an inverted multicasting is achieved.

3. Result and Discussion

The experimental set-up for wavelength multicasting is shown in Fig. 4. The placement of the control and signal wavelength is labelled in Fig. 3(b). The extinction and Q-factor of the control and four signals are (27.8 dB, 7,000), (10.95 dB, 11,300), (14.11 dB, 9,100), (13.27 dB, 9,300) and (10.9 dB, 11,700) respectively. A Control is modulated with $2^{15} - 1$ pseudo-random bit stream and amplified using an EDFA followed by a bandpass filter (BPF). The control optical power is tuned by changing the EDFA current and BPF is used to suppress the spontaneous emission noise from the EDFA. Once the minimum power required to achieve multicasting is determined, the EDFA current is fixed to maintain the signal-to-noise ratio from the EDFA throughout the experiment. The control is then combined with the four signal wavelength using a 90:10 coupler and finally coupled to the device using a grating coupler. A control power of 0 dBm and a signal power of -12 dBm is used just before the grating couplers. At the output, the control and signals were amplified again using an EDFA and the control is filtered using a bandstop filter. The filtered signal is analysed using a digital oscilloscope after passing it through PD. The time domain sampling oscilloscope used has an electrical bandwidth of 20 GHz and the PD used before the oscilloscope also has a bandwidth of 20 GHz. A variable optical attenuator is used after the BPF for BER measurements. Bit error rate is measured with BERT where the bit pattern generated by multicasting is compared with the original bit stream to quantify the bit error.

Fig. 5 shows the multicast output for the four signals for both, inverted and non-inverted cases, at 1.8 Gbps. The optical swing of the bit pattern after the 90:10 splitter is 30 dB where bit '1' has

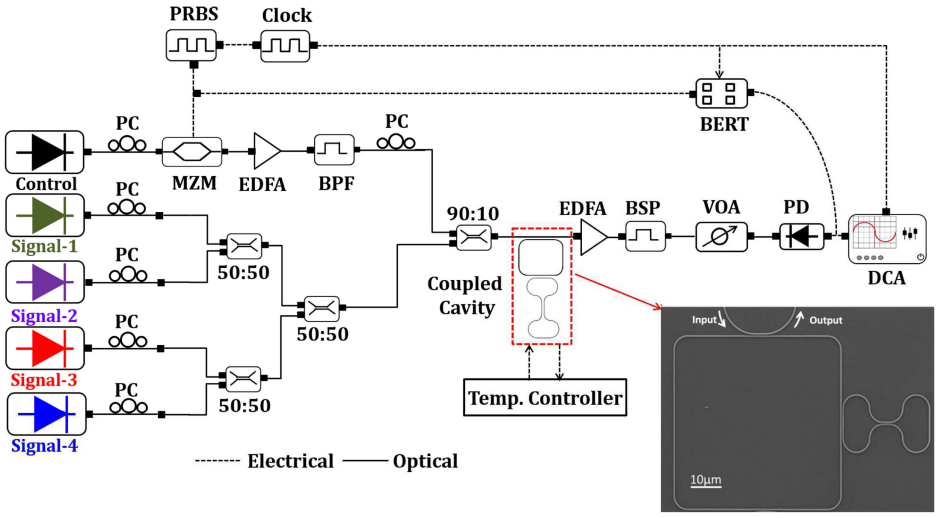

Fig. 4. Experimental setup for wavelength multicasting along with the SEM image of fabricated device. MZM: Mach-Zehnder modulator, PRBS: pattered random bit sequence. EDFA: erbirum doped fiber amplifier, BPF: band pass filter, BSP: band stop filter, PC: polarization controller, VOA: variable optical attenuator, PD: photo-detector, DCA: digital communication analyzer, and BERT: bit error rate tester.

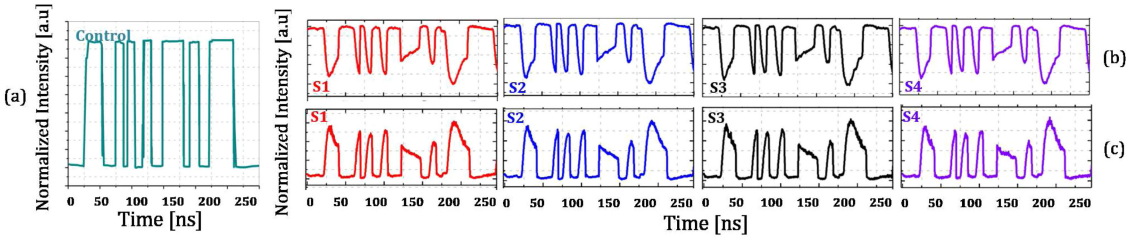

Fig. 5. (a) Control bit pattern and four channel multicasting for (b) inverted and (c) non-inverted signal. The data rate is 1.8 Gbps (S: signal).

0 dBm of optical power and bit '1' has −30 dBm of optical power. The on-off extinction of the non-inverted signal is 12.2 dB whereas for the inverted signal it is 16.7 dB. It has been noted from the multicast output that the shape distortion of the isolated '1' is more severe than consecutive bit '1'. The distortion can be attributed to the free carrier lifetime and the bit rate. Since isolated '1's have shorter extinction duration compared to successive '1's, the extinction of isolated '1's is observed to be lower than the successive '1's. Furthermore, with successive '1's we observe distortion in the pulse shape due to higher recombination then generation rate. The distortion of isolated '1's will be even more severely affected when the frequency of operation is much larger than the carrier generation frequency, which is observed in high data rate and signal quality characterisation presented in the following section.

Fig. 6(a) shows the eye diagram for the four channels operating at 1.8 Gbps and Fig. 6(c) shows the corresponding BER for the channels. Eyes were measured after calculating the BER and determining the regime for error free operation. The eye remains wide open for all the channels. The BER also remains almost same with a power variation of around 1 dB for error-free operation, and this is attributed to extinction difference between the channels. We take standard error-free transmission as 1-bit error in 10^9 bits. With increasing data rate we could observe degradation in the eye beyond 12 Gbps (Fig. 6(b)). The same is observed in BER power penalty plot in Fig. 6(d). BER degrades progressively with data rate. However, even at 12 Gbps, the BER is above the Forward Error Correction (FEC) limit. With this demonstration, we present for the first time an FCA assisted multicasting in Si operating at an aggregated data rate of 48 Gbps (4×12 Gbps).

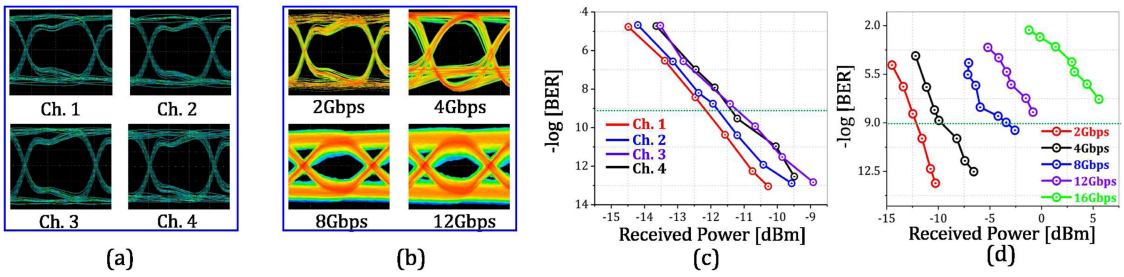

Fig. 6. (a) and (c) Eye diagram and bit error rate measurements at 1.8 Gbps. (b) and (d) Measurements for higher frequencies are provided.

TABLE 1

Overview of Reported Integrated Multicasting Solutions on Various Material Platforms and Exploiting Various Material Platforms and Mechanisms. SOA: Semiconductor Optical Amplifier

Ref.	Architecture	Aggregate Data Rate (Gbps)	Mechanism	Material Plat-form
2	MRR Array	10	Thermal	Silicon
10	Waveguide	10	All-Optical	Silicon
29	SOA	40	All-Optical	InP
30	MRR	20	All-Optical	Si_3N_4
31	Waveguide	22	All-Optical	Silicon
32	MRR Array	10	Thermal	Silicon
33	Waveguide	36	All-Optical	Silicon
34	Waveguide	10	All-Optical	Silicon
35	Waveguide	10	All-Optical	Silicon
This Work	Coupled MRR	48	All-Optical	Silicon

Finally, a table has been provided for comparison between different types of integrated architectures reported for multicasting. Table 1 reports architecture, aggregate data rate, mechanism used for carrying out multicasting and the substrate material over which the devices were fabricated.

4. Conclusion

In conclusion, we have experimentally demonstrated wavelength multicasting using a coupled Si coupled microring resonator. A quadruple resonance splitting is achieved in a coupled MRR system that is closely spaced with high-quality factor. We have shown tunable nature of the splitting as well. The split resonance along with the unperturbed resonance is utilised to demonstrate wavelength multicasting by exploring TPA induced free carrier dispersion in the cavity. We have demonstrated an aggregate data rate of 48 Gbps (4 $\times$ 12 Gbps). A detailed signal analysis is also presented. The single-channel data rate could be further increased by reducing the carrier lifetime though incorporation of defect states. However, this would have a direct implication on the absorption loss, signal extinction and TPA threshold. Hence, a compromise between speed, loss and signal integrity is inevitable.

Acknowledgment

The authors would like to thank the supporting facilities at CeNSE, Indian Institute of Science, Bengaluru.

References

[1] X. Wang, L. Huang, K. Yi, X. Feng, and S. Gao, "All-optical wavelength conversion and five-channel multicasting for 20 Gbit/s QPSK signals in a silicon waveguide," *Opt. Lett.*, vol. 39, no. 21, pp. 6122–6125, 2014.
[2] A. Gazman *et al.*, "Software-defined control-plane for wavelength selective unicast and multicast of optical data in a silicon photonic platform," *Opt. Exp.*, vol. 25, no. 1, pp. 232–242, 2017.
[3] S. J. B. Yoo, "Wavelength conversion technologies for WDM network applications," *J. Lightw. Technol.*, vol. 14, no. 6, pp. 955–966, Jun. 1996.
[4] C. S. Bres *et al.*, "Parametric photonic channelized RF receiver," *IEEE Photon. Technol. Lett.*, vol. 23, no. 6, pp. 344–346, Mar. 2011.
[5] S. Khaleghi *et al.*, "High-speed correlation and equalization using a continuously tunable all-optical tapped delay line," *IEEE Photon. J.*, vol. 4, no. 4, pp. 1220–1235, Aug. 2012.
[6] W. Zhang, H. Wang, and K. Bergman, "Next-generation optically-interconnected high-performance data centers," *J. Lightw. Technol.*, vol. 30, no. 24, pp. 3836–3844, Dec. 2012.
[7] I. Aldaya, A. Gil-Molina, J. L. Pita, L. H. Gabrielli, H. L. Fragnito, and P. Dainese, "Nonlinear carrier dynamics in silicon nano-waveguides," *Optica*, vol. 4, no. 10, pp. 1219–1227, 2017.
[8] W. Astar *et al.*, "Tunable wavelength conversion by XPM in a silicon nanowire, and the potential for XPM-multicasting," *J. Lightw. Technol.*, vol. 28, no. 17, pp. 2499–2511, Sep. 2010.
[9] A. Biberman *et al.*, "Wavelength multicasting in silicon photonic nanowires," *Opt. Exp.*, vol. 18, no. 17, pp. 18047–18055, 2010.
[10] H. F. Ting *et al.*, "Wavelength multicasting through four-wave mixing with an optical comb source," *Opt. Exp.*, vol. 25, no. 8, pp. 9276–9284, 2017.
[11] J. Qin, Y. Ji, H. Wang, D. Wang, M. Zhang, and G.-W. Lu, "Multichannel wavelength multicasting for two QPSK signals based on FWM in SOA," *Chin. Opt. Lett.*, vol. 13, no. 1, 2015, Art. no. 010601.
[12] D. Wang *et al.*, "Performance comparison of using SOA and HNLF as FWM medium in a wavelength multicasting scheme with reduced polarization sensitivity," *J. Lightw. Technol.*, vol. 28, no. 24, pp. 3497–3505, Dec. 2010.
[13] A. Bazin *et al.*, "Ultrafast all-optical switching and error-free 10 Gbit/s wavelength conversion in hybrid InP-silicon on insulator nanocavities using surface quantum wells," *Appl. Phys. Lett.*, vol. 104, no. 1, 2014, Art. no. 011102.
[14] S. F. Preble, Q. Xu, B. S. Schmidt, and M. Lipson, "Ultrafast all-optical modulation on a silicon chip," *Opt. Lett.*, vol. 30, no. 21, pp. 2891–2893, 2005.
[15] Q. Li, Z. Zhang, F. Liu, M. Qiu, and Y. Su, "Dense wavelength conversion and multicasting in a resonance-split silicon microring," *Appl. Phys. Lett.*, vol. 93, no. 8, 2008, Art. no. 081113.
[16] M. C. M. M. Souza, L. A. M. Barea, F. Vallini, G. F. M. Rezende, G. S. Wiederhecker, and N. C. Frateschi, "Embedded coupled microrings with high-finesse and close-spaced resonances for optical signal processing," *Opt. Exp.*, vol. 22, no. 9, pp. 10430–10438, 2014.
[17] Q. Li *et al.*, "Influence of two-photon absorption on the dynamic behaviors of microring resonators," *Appl. Opt.*, vol. 56, no. 10, pp. 2580–2588, 2017.
[18] R. M. Osgood *et al.*, "Engineering nonlinearities in nanoscale optical systems: Physics and applications in dispersion-engineered silicon nanophotonic wires," *Adv. Opt. Photon.*, vol. 1, no. 1, pp. 162–235, 2009.
[19] X. Sang, E. K. Tien, and O. Boyraz, "Applications of two photon absorption in silicon," *J. Optoelectron. Adv. Mater.*, vol. 11, no. 1, pp. 15–25, 2008.
[20] Q. Lin, O. J. Painter, and G. P. Agrawal, "Nonlinear optical phenomena in silicon waveguides: Modeling and applications," *Opt. Exp.*, vol. 15, no. 25, pp. 16604–16644, 2007.
[21] A. Pandey and S. K. Selvaraja, "Tunable coupling-induced resonance splitting in self-coupled silicon ring cavity with robust spectral characteristics," *Opt. Lett.*, vol. 42, no. 14, pp. 2854–2857, 2017.
[22] G. Gao *et al.*, "Tuning of resonance spacing over whole free spectral range based on Autler-Townes splitting in a single microring resonator," *Opt. Exp.*, vol. 23, no. 21, pp. 26895–26904, 2015.
[23] H. Yu, P. Li, M. Chen, H. Chen, S. Yang, and S. Xie, "Analog photonic link based on the Aulter-Townes splitting induced dual-band filter for OCS and the SOI signal processor," *Opt. Lett.*, vol. 40, no. 10, pp. 2225–2228, 2015.
[24] J. Wu *et al.*, "On-chip tunable second-order differential-equation solver based on a silicon photonic mode-split microresonator," *J. Lightw. Technol.*, vol. 33, no. 17, pp. 3542–3549, Sep. 2015.
[25] J. Wu *et al.*, "Passive silicon photonic devices for microwave photonic signal processing," *Opt. Commun.*, vol. 373, pp. 44–52, 2016.
[26] Q. Li, T. Wang, Y. K. Su, M. Yan, and M. Qiu, "Coupled mode theory analysis of mode-splitting in coupled cavity system," *Opt. Exp.*, vol. 18, no. 8, pp. 8367–8382, 2010.
[27] Y. Xu, Y. Li, R. K. Lee, and A. Yariv, "Scattering-theory analysis of waveguide-resonator coupling," *Phys. Rev. E*, vol. 62, no. 5, pp. 7389–7404, 2000.
[28] Q. Xu, V. R. Almeida, and M. Lipson, "Micrometer-scale all-optical wavelength converter on silicon," *Opt. Lett.*, vol. 30, no. 20, pp. 2733–2735, 2005.
[29] X. Zheng, N. Calabretta, O. Raz, D. Zhao, R. Lu, and Y. Liu, "40 Gb/s all-optical unicast and multicast wavelength converter array on an InP monolithically integrated chip fabricated by MPW technology," *Opt. Exp.*, vol. 25, no. 7, pp. 7616–7626, 2017.

[30] C. Bao *et al.*, "Demonstration of optical multicasting using Kerr frequency comb lines," *Opt. Lett.*, vol. 41, no. 16, pp. 3876–3879, 2016.
[31] M. Chagnon, M. Spasojevic, R. Adams, J. Li, D. V. Plant, and L. R. Chen, "Wavelength multicasting at 22-Gbaud 16-QAM in a silicon nanowire using four-wave mixing," *IEEE Photon. Technol. Lett.*, vol. 27, no. 8, pp. 860–863, Apr. 2015.
[32] Z. Su, E. Timurdogan, M. Moresco, G. Leake, D. D. Coolbaugh, and M. R. Watts, "Wavelength routing and multicasting network in ring-based integrated photonics," in *Proc. Adv. Photon. OSA Tech. Dig.*, 2015, Paper IT4A.3.
[33] X. Wang, L. Huang, and S. Gao, "Low-power-penalty wavelength multicasting for 36 Gbit/s 16-QAM coherent optical signals in a silicon waveguide," *Opt. Lett.*, vol. 39, no. 24, pp. 6907–6910, 2014.
[34] M. Pu *et al.*, "Polarization insensitive wavelength conversion in a dispersion-engineered silicon waveguide," *Opt. Exp.*, vol. 20, no. 15, pp. 16374–16380, 2012.
[35] M. Pu *et al.*, "One-to-six WDM multicasting of DPSK signals based on dual-pump four-wave mixing in a silicon waveguide," *Opt. Exp.*, vol. 19, no. 24, pp. 24448–24453, 2011.